

## 基于波长调制腔增强吸收光谱技术的 CO 体积分数测量

王宣, 高光珍<sup>\*\*</sup>, 龙芳宇, 杨玉冰, 蔡廷栋<sup>\*</sup>

江苏师范大学物理与电子工程学院, 江苏 徐州 221116

**摘要** 基于腔增强吸收光谱(CEAS)技术和波长调制光谱(WMS)技术,搭建了腔增强光谱测量系统,并采用该系统实现了CO体积分数的测量。实验中使用中心波长为2.3 μm的分布式反馈激光器作为光源,以反射率为99.8%的两片高反镜构建了基长为30 cm的光学腔,达到了147.15 m的有效吸收路径;在此基础上,利用4297.705 cm<sup>-1</sup>处的CO吸收谱线作为传感目标,实现了对CO的探测。利用CO体积分数不同的CO+N<sub>2</sub>的混合气体对系统的测量准确度进行验证,结果显示,测量值与参考值大小基本吻合,测量误差约为0.2%,证实了所搭建系统的测量准确性。利用体积分数为3×10<sup>-6</sup>的CO气体的二次谐波信号对系统的探测极限进行了分析,得到系统对CO的探测极限为138×10<sup>-9</sup>。

**关键词** 光谱学; 腔增强吸收光谱技术; 波长调制光谱; CO气体; 体积分数测量

中图分类号 O433.1

文献标志码 A

DOI: 10.3788/CJL221416

## 1 引言

CO是无色无味、有毒且可燃的气体,吸入过量CO会引起组织缺氧,使人体器官功能受损,尤其是耗氧量高的大脑会随着缺氧时间延长而发生水肿坏死,甚至出现脑死亡。大气环境中CO的主要来源是机动车尾气和工业不完全燃烧产生的废气。随着世界工业化的发展,环境污染问题愈发严重,CO污染也愈发明显。为了能够有效控制CO气体的排放,需要对CO气体浓度进行实时精确检测。

近些年来,在检测气体方面,光学检测技术凭借其相对较低的系统成本、较高的可靠性以及可持续性获得了广泛关注与研究。该方法同样适用于CO浓度的检测,但目前的研究大多是基于吸收光谱理论展开的,较为常见的光学检测技术有非分散红外技术<sup>[1-2]</sup>(NDIR技术)、傅里叶变换红外光谱技术<sup>[3-4]</sup>(FTIR技术)、光腔衰荡光谱技术<sup>[5-6]</sup>(CRDS技术)以及可调谐半导体激光吸收光谱技术<sup>[7-10]</sup>(TDLAS技术)。其中:非分散红外技术具有仪器结构简单、测量精度高等优点,但在测量过程中会受到背景气体的干扰,检测结果受到一定影响;傅里叶变换红外光谱技术具有分辨率高、精确度高以及波段宽等优点,但其定量分析的准确度较低,在成分检测的应用中存在着许多限制。相较于以上几种检测技术,可调谐半导体激光吸收光谱技

术具有高灵敏度、高分辨率、快速响应、不受背景气体干扰等优点,而且气室具有结构简单、成本低、维护方便、使用寿命长等特点。

在一系列提高可调谐半导体激光吸收光谱技术检测灵敏度的方法中,与长光程吸收池<sup>[11-12]</sup>结合的方法是最为直接的。为了实现长光程,一般用怀特池<sup>[13-15]</sup>进行多通吸收,但在反射过程中会出现光能量损失的情况,能够反射的次数有限,而且怀特池的有效光程有限,当待测CO气体浓度很低时,其测量精度不足以进行有效检测。腔增强吸收光谱技术(CEAS技术)<sup>[16-20]</sup>由于光在高反镜构成的腔内发生多次反射而具有极长的有效吸收光程,测量灵敏度高,能够实现对极低浓度CO的检测。

笔者在自行搭建的高精度光学积分腔的基础上,以2.3 μm分布式反馈激光器(DFB激光器)作为光源,开发了一套CO腔增强吸收光谱测量系统,并结合波长调制吸收光谱技术(WMS技术),以位于4297.705 cm<sup>-1</sup>处的CO谱线作为传感目标,实现了对CO体积分数的灵敏度探测。

## 2 吸收光谱理论

### 2.1 波长调制吸收光谱

波长调制技术<sup>[21-23]</sup>利用可调谐激光器的波长可调谐特性来降低低频噪声,从而提高灵敏度。该技术的

收稿日期: 2022-11-14; 修回日期: 2022-12-13; 录用日期: 2023-02-08; 网络首发日期: 2023-02-18

基金项目: 国家自然科学基金(42275136, 62275110, 61875079, 61805110, 61475068, 11104237)、江苏省碳达峰碳中和科技创新专项资金(BE2022314)、江苏省重点研发计划(社会发展)专项资金(BE2021634)、江苏师范大学研究生科研与实践创新计划(2022XKT1346)

通信作者: \*caitingdong@126.com; \*\*ggz@jsnu.edu.cn

基本工作原理:采用低频电流扫描激光器,从而扫过气体吸收线,得到该气体的吸收信号,然后加入高频正弦调制信号,调制激光器的发光波长,在周期性调制信号下使用锁相放大器提取所需谐波信号。

当向二极管激光器注入频率为  $f$  的正弦波对电流进行调制时,激光器的瞬时频率以及对应的激光强度同时发生变化。激光通过待测吸收池后,得到的透射激光强度为  $I_1(t)$ ,其遵循 Beer-Lambert 定律,可表示为

$$I_1(t) = I_0(t) \cdot \tau [\bar{\nu} + a \cos(\omega t)] \approx I_0(t) \left\{ 1 - \alpha [\bar{\nu} + a \cos(\omega t)] \right\}, \quad (1)$$

式中:  $\tau$  为激光透射系数;  $\bar{\nu}$  为激光的中心频率;  $a$  为调制振幅,  $\text{cm}^{-1}$ ;  $\omega = 2\pi f$ ;  $\alpha$  为吸收系数;  $t$  为时间; 入射光强  $I_0(t) = \bar{I}_0 [1 + i_0 \cos(2\pi ft + \psi_1) + i_2 \cos(4\pi ft + \psi_2)]$ , 其中的  $\bar{I}_0$  为中心频率处的平均光强,  $i_0, i_2$  分别为线性和非线性激光强度调制(IM)振幅,  $\psi_1$  和  $\psi_2$  分别表示线性频率调制与激光强度调制之比的相移以及非线性频率调制与激光强度调制之比的相移。

对输出信号进行余弦傅里叶级数展开得到

$$\alpha [\bar{\nu} + a \cos(\omega t)] = - \sum_{k=0}^{\infty} H_k(\bar{\nu}, a) g \cos(k\omega t), \quad (2)$$

将吸收系数  $\alpha(\nu) = PXS(T)\Phi\nu L$  代入式(2),得到傅里叶系数的表达式为

$$H_0(\bar{\nu}, a) = - \frac{PS(T)XL_{\text{eff}}}{2\pi} \int_{-\pi}^{\pi} \varphi(\bar{\nu} + a \cos \theta) d\theta, \quad (3)$$

$$H_k(\bar{\nu}, a) = - \frac{PS(T)XL_{\text{eff}}}{\pi} \int_{-\pi}^{\pi} \varphi(\bar{\nu} + a \cos \theta) \cos(k\theta) d\theta, \quad (4)$$

式中:  $P$  为压强;  $S(T)$  为线强度;  $X$  为吸收组分的体积分数;  $\Phi$  为吸收谱线的线型函数;  $L_{\text{eff}}$  为谐振腔的有效光程;  $\varphi$  为调制相位;  $k$  为谐波次数;  $\nu$  为激光的中心频率。

由此可以看出,调制振幅、吸收组分的体积分数、线强以及线型函数等参数都会对谐波信号产生影响。另外,在实验过程中,通常使用二次谐波信号( $2f$ )进行气体浓度的检测,其原因是二次谐波信号是偶次谐波信号,其峰值处于吸收线的中心位置,且在偶次谐波信号中是最强的信号。另外,在波长调制吸收光谱技术中,采集到的二次谐波信号一般是由锁相放大器对探测器信号进行解调得到的,通常假设探测器与参考信号之间的相移为 0,因此可得到与探测相移无关的二次谐波信号的幅值为

$$R_{2f} = \sqrt{X_{2f}^2 + Y_{2f}^2} = \frac{G\bar{I}_0}{2} \left\{ \left[ H_2 + \frac{i_0}{2} (H_1 + H_3) \cos \psi_1 + i_2 \left( 1 + H_0 + \frac{H_4}{2} \right) \cos \psi_2 \right]^2 + \left[ H_2 + \frac{i_0}{2} (H_1 - H_3) \sin \psi_1 + i_2 \left( 1 + H_0 - \frac{H_4}{2} \right) \sin \psi_2 \right]^2 \right\}^{\frac{1}{2}}, \quad (5)$$

式中:  $G$  为系统的光电增益;  $H_i$  为  $i$  次谐波的傅里叶系数;  $X_{2f}, Y_{2f}$  分别为二次谐波信号的分量。

由于  $R_{2f}$  与吸收组分的体积分数不成正比,在吸收为零时  $X_{2f}^0$  和  $Y_{2f}^0$  分量不为零,因此无吸收时二次谐波背景信号的振幅为

$$R_{2f}^0 = \frac{G\bar{I}_0}{2} i_{20} \quad (6)$$

从  $X_{2f}$  和  $Y_{2f}$  中去除背景信号,得到只与吸收有关的二次谐波信号为

$$S_{2f} = \sqrt{(X_{2f} - X_{2f}^0)^2 + (Y_{2f} - Y_{2f}^0)^2} = \frac{G\bar{I}_0}{2} \left\{ \left[ H_2 + \frac{i_0}{2} (H_1 + H_3) \cos \psi_1 + i_2 \left( H_0 + \frac{H_4}{2} \right) \cos \psi_2 \right]^2 + \left[ \frac{i_0}{2} (H_1 - H_3) \sin \psi_1 + i_2 \left( H_0 - \frac{H_4}{2} \right) \sin \psi_2 \right]^2 \right\}^{1/2}. \quad (7)$$

由此可以得到被测气体的体积分数与其二次谐波信号幅值之间存在一定的线性关系,所以在实验过程中通常用二次谐波信号的幅值来表征气体的体积分数。

### 2.2 腔增强吸收光谱技术

腔增强吸收光谱技术中的腔是由两个具有高反射率(反射率  $R > 99\%$ )的镜片组成的,可以将其看成是一个法布里-珀罗腔(F-P腔)。激光在腔内多次反射,腔内损耗为  $L$ ,两侧高反镜(M1和M2)的反射率均为  $R$ ,系统的腔长为镜片之间的距离用  $d$  (cm)表示,在实验中一般忽略掉腔镜中的损耗。

每一次出射的光强均可推导出来。

由规律分析可得第  $n$  次的出射光强  $I_n$  为

$$I_n = I(1 - R)(1 - L)R^{(n-1)}(1 - L)^{(n-1)}R^{(n-1)}(1 - L)^{(n-1)}(1 - R) = I_1 [R^2(1 - L)^2]^{n-1}, \quad (8)$$

式中:  $I$  为入射光强。

F-P腔的总出射光强是每一次出射光强的总和,因此总出射光强 $I_s$ 可以表示为

$$I_s = I_1 + I_2 + I_3 + I_4 + \dots + I_n = \frac{I(1-R)^2(1-L)}{1-R^2(1-L)^2} \quad (9)$$

当腔内无吸收介质( $L=0$ )时,透射光强为 $I_0 = I(1-R)/(1+R)$ ,此时可得到

$$\frac{I_0}{I_s} = \frac{1-R^2(1-L)^2}{(1-R^2)(1-L)^2} \quad (10)$$

忽略其他损耗,只考虑由介质吸收引起的损耗,也就是说, $1-L = \exp(-\alpha d)$ ,则可得到吸收系数 $\alpha$ 为

$$\alpha = \frac{1}{d} \ln \left| \frac{\sqrt{[(I_0/I_s)(1-R^2)]^2 + 4R^2} - (I_0/I_s)(1-R^2)}{2R^2} \right| \quad (11)$$

在光学腔中,当 $R$ 趋近于1时,对式(11)进行化简可得吸收系数近似为

$$\alpha \approx \frac{1}{d} \left( \frac{I_0}{I_s} - 1 \right) (1-R) \quad (12)$$

另外,结合Beer-Lambert定律与式(12)可得出光学腔的有效吸收光程 $L_{\text{eff}}$ 为

$$L_{\text{eff}} = \frac{d}{1-R} \quad (13)$$

### 3 实验结果与分析

#### 3.1 谱线选择

对于气体体积分数的检测来说,选择合适的谱线尤为重要。图1是根据HITRAN 2016数据库信息给出的300 K温度下CO、CO<sub>2</sub>以及H<sub>2</sub>O在1~5 μm波段范围内的吸收线强。可见,2.3 μm波段附近存在CO的吸收谱线,虽然与4~5 μm波段范围的CO相比,其吸收弱2~3个数量级,但结合波长调制光谱以及腔增强吸收光谱等灵敏探测技术,仍能够达到较好的探测灵敏度。与4~5 μm波段范围相比,2.3 μm波段使用的半导体激光器、探测器以及其他光学元件具有价格更为低廉、实验设备成本较低以及使用过程中的操作更为方便等优点,考虑到这一点,选择2.3 μm DFB二极管激光器作为光源。

为了避免其他气体分子的干扰,选择了一条相对孤立且具有较高吸收线强的CO吸收线作为传感目

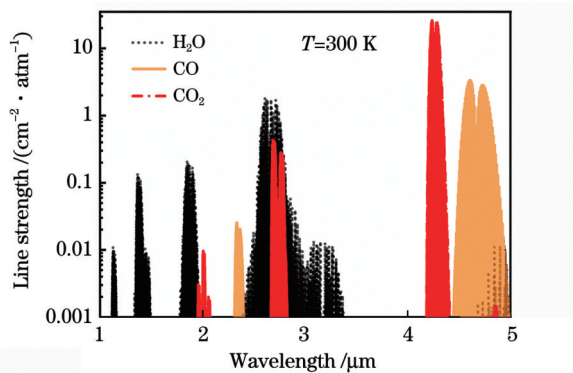


图1 300 K温度下1~5 μm波段CO、CO<sub>2</sub>和H<sub>2</sub>O的谱线分布  
Fig. 1 Spectral line distribution of CO, CO<sub>2</sub> and H<sub>2</sub>O in the wavelength range of 1-5 μm at 300 K

标。基于HITRAN 2016数据库中4288~4302 cm<sup>-1</sup>范围内谱线的具体参数,利用Voigt线型模拟了体积分数分别为10<sup>-7</sup>的CO、2×10<sup>-7</sup>的CH<sub>4</sub>、10<sup>-3</sup>的CO<sub>2</sub>以及10<sup>-3</sup>的H<sub>2</sub>O分子的吸收谱线,模拟结果如图2所示。在4288~4302 cm<sup>-1</sup>范围内,大部分波段上H<sub>2</sub>O气体的吸收都比较强烈;而在4297.7 cm<sup>-1</sup>附近CO有较强吸收,无CO<sub>2</sub>气体分子的吸收,H<sub>2</sub>O和CH<sub>4</sub>存在吸收但线强相对较低,对CO测量的影响较小。此外,图2中给出了利用三阶多项式对激光器工作温度为25 °C时的注入电流与波数的精确拟合结果,结果显示,4297.705 cm<sup>-1</sup>处的CO谱线非常适合在大气中进行探测。

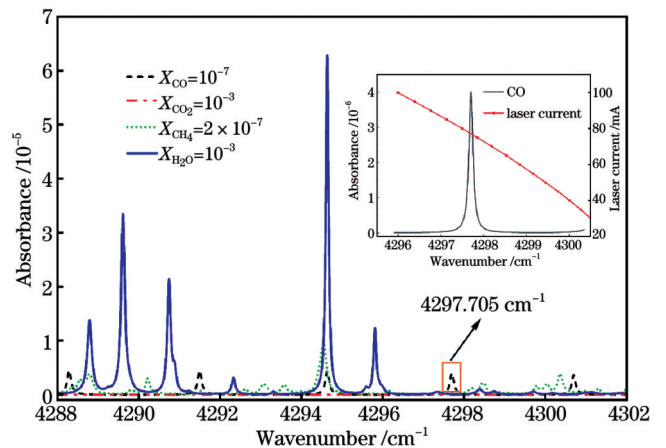


图2 4288~4302 cm<sup>-1</sup>范围内CO、CO<sub>2</sub>、CH<sub>4</sub>和H<sub>2</sub>O的谱线分布情况以及25 °C下DFB激光器电流与波数的关系  
Fig. 2 Spectral line distributions of CO, CO<sub>2</sub>, CH<sub>4</sub> and H<sub>2</sub>O in 4288-4302 cm<sup>-1</sup> and current-wavenumber relationship of DFB laser at 25 °C

#### 3.2 腔镜反射率以及有效吸收光程的标定

实验前对腔镜在2.3 μm处的反射率以及有效吸收光程进行了标定,标定方法为:向多通池以及谐振腔中通入等量且CO体积分数均为50×10<sup>-6</sup>的CO+N<sub>2</sub>混合气体,同时对两个不同测量装置中的CO气体的吸收信号进行探测。分别获得所选的CO谱线的吸收光谱信号,对信号进行积分得到光学腔与多通池的积分面积。由 $\frac{A_{\text{CEAS}}}{A_{\text{MP}}} = \frac{L_{\text{eff}}}{L_{\text{MP}}}$ 可知光学腔与多通池的光程之比等于二者积分面积之比,式中, $A_{\text{CEAS}}$ 和 $A_{\text{MP}}$ 分别为

光学腔和多通池的积分面积,  $L_{\text{eff}}$  和  $L_{\text{MP}}$  分别为光学腔和多通池的有效光程。已知本实验开放光路中多通池的光程为 28.8 m, 由此可以得到本实验中离轴腔的有效吸收光程为 147.15 m。再根据式  $L_{\text{eff}} = \frac{d}{1-R}$  ( $L_{\text{eff}}$  为光学腔的有效光程,  $d$  为光学腔的腔长,  $R$  为腔镜的反射率) 得到腔镜在  $2.3 \mu\text{m}$  处的反射率为 99.8%, 这一结果与镜片生产厂家所给数据基本一致, 表明了本次实验的准确性。

### 3.3 最佳调制振幅

在波长调制技术中, 二次谐波信号的幅值会受到调制振幅的影响。为了得到最佳的二次谐波信号, 需要确定最为合适的调制振幅。本文利用 CO 气体的吸收谱线确定调制振幅的最佳值, 方法为: 选用波数为  $4297.705 \text{ cm}^{-1}$  的谱线在常温常压环境下进行测量。向实验用密封箱内通入 CO 体积分数为 1% 的 CO + N<sub>2</sub> 混合气体, 在调节前设定函数发生器的三角波频率为 2 Hz, 振幅为 1.54 V, 同时将锁相放大器提供的正弦波频率固定在 880 Hz。随后在一定范围内调节正弦波的振幅, 得到不同质量的信号并将其用于后续的分析选择。调节结果如图 3 所示, 图中所示为 200~430 mV 调制振幅范围内得到的二次谐波信号的幅值。可见, 二次谐波信号的幅值会随着调制振幅的增大而先增大后减小, 二次谐波信号的幅值存在一个最大值, 该值对应的最佳调制振幅为 360 mV, 对应的调制波数

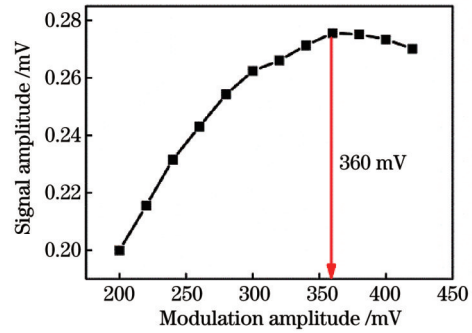


图 3 CO 气体在不同调制振幅下的二次谐波信号幅值  
Fig. 3 Second harmonic signal amplitude of CO gas under different modulation amplitudes

为  $0.1261 \text{ cm}^{-1}$ 。

## 4 实验装置

图 4 为本次实验中搭建的密封式 CO 腔增强测量系统。实验所使用的  $2.3 \mu\text{m}$  DFB 激光器的生产厂家为 Nanoplus, 该激光器输出激光的线宽小于 3 MHz, 典型功率为 6 mW, 能够满足本实验的需求。密封箱内的光学腔由两片高反镜组成, 腔长为 30 cm。装置中所使用的高反镜的直径为 25.4 mm, 曲率半径为 1 m, 其在  $1.9\sim 2.3 \mu\text{m}$  波长范围内的反射率可达到 99.8%。在整个系统中, 准直头、高反镜、透镜以及探测器固定在光学平板上, 以便确保系统的一致性。腔增强系统

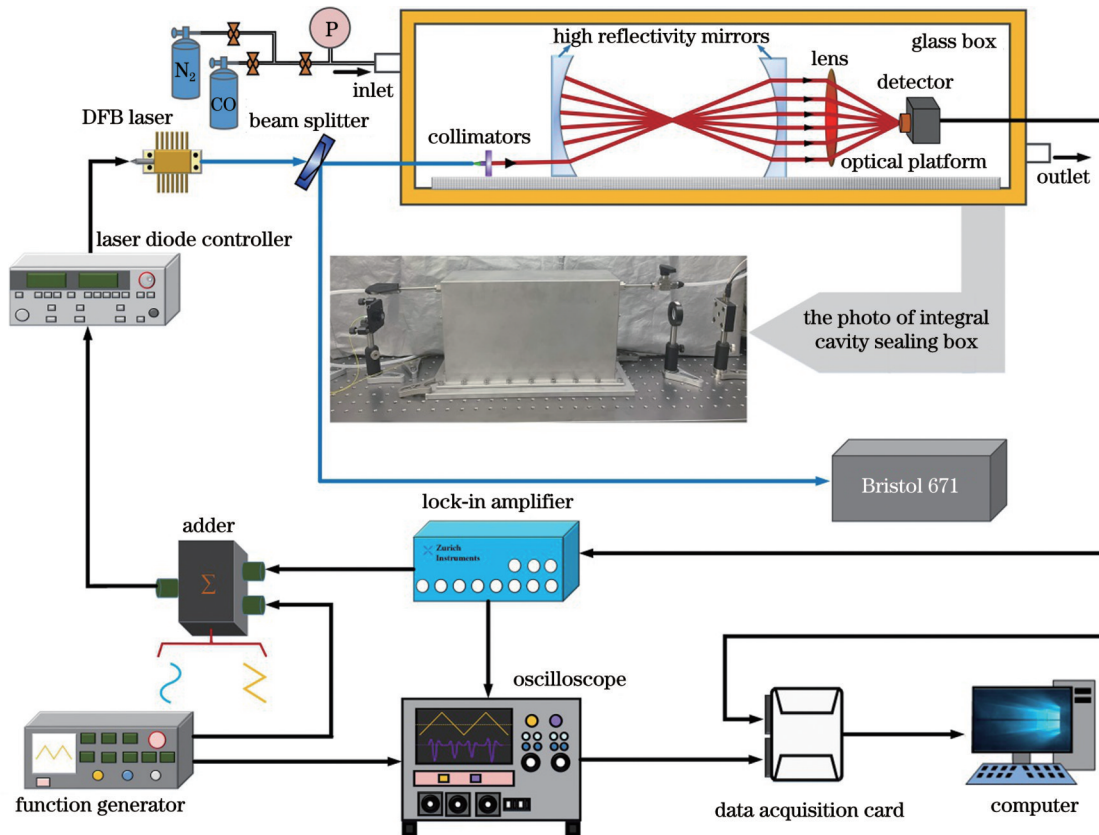


图 4 实验装置示意图  
Fig. 4 Schematic of the experimental device

外面的密封箱由铝合金制成, 体积为  $2.7 \text{ dm}^3$ , 其进气口和出气口分别设置在密封箱的左右两侧, 以便保证气体的流动性测量。

实验中所用  $2.3 \text{ }\mu\text{m}$  DFB 激光器输出的激光被光纤分束器分为两部分, 其中: 一部分通入到波长计 (Bristol 671) 中, 以便在实际测量前确定激光器的中心波长; 另一部分通入到铝合金密封箱中, 以便实现对测气体的测量。激光光束通过密封箱进入光学腔内, 在腔内多次反射后从另一端透射出腔, 再经由焦距为  $5 \text{ mm}$  的透镜会聚进入 InGaAs 探测器中进行探测。探测器信号被送入到锁相放大器输入端口, 根据具体的参数设置对信号进行解调, 解调方式为单相解调, 解调后的信号用数据采集卡 (National Instruments USB-6361) 进行采集并存储在计算机中, 以便进行后续数据处理。函数发生器产生的频率为  $2 \text{ Hz}$  的三角波和锁相放大器产生的频率为  $880 \text{ Hz}$  的正弦波被加法器叠加在一起, 该叠加信号被送入激光控制器, 以实现激光波长的扫描和调制。

## 5 系统测量准确度的验证

### 5.1 CO 波长调制吸收光谱的测量

基于该系统开展了 CO 气体二次谐波信号的测量实验, 以验证本实验系统的测量准确性。选择了 CO 体积分数不同的 CO+N<sub>2</sub> 混合气体进行实验, 分别将预先已经配制好的 CO+N<sub>2</sub> 的混合气体通入密封箱内进行测量。在 CO+N<sub>2</sub> 混合气体通入密封箱内之前, 先用高纯 N<sub>2</sub> (纯度为 99.999%) 对密封箱进行冲洗, 以保证前一次测量的残留气体被充分排出箱内, 防止对下一次实验产生影响。实验在  $101325 \text{ Pa}$ 、 $300 \text{ K}$  的固定条件下进行, 分别测量了体积分数不同 ( $3 \times 10^{-6}$ 、 $10 \times 10^{-6}$ 、 $30 \times 10^{-6}$ 、 $50 \times 10^{-6}$ ) 的 CO 的二次谐波信号, 二次谐波信号如图 5 所示。图 6 给出了各体积分数 CO 的二次谐波信号的峰值高度与体积分数之间的线性关系, 拟合结果显示各数据点之间的线性度  $R^2=0.998$ , 相对标准偏差为  $0.34\%$ 。由此可知在本次实验所测量的 CO 体积分数范围内二次谐波信号的峰值高

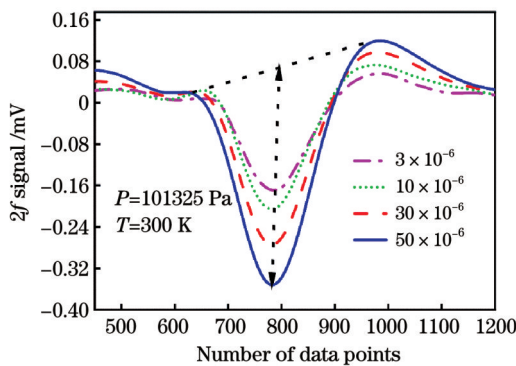


图 5 不同体积分数 CO 气体的二次谐波信号

Fig. 5 Second harmonic ( $2f$ ) signal of CO gas with different volume fractions

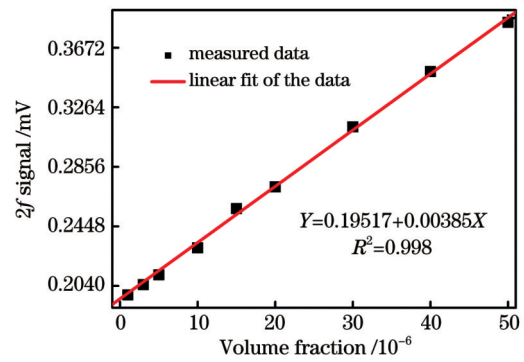


图 6 二次谐波信号幅值与 CO 体积分数之间的线性关系

Fig. 6 Linearity between second harmonic signal amplitude and CO volume fraction

度与 CO 体积分数保持着良好的线性关系。存在误差的主要原因是密封箱内依旧存在部分气体残留以及实验时压力表的读数误差。

为了验证实验测量的准确性与可行性, 将 CO 体积分数的测量值与已知参考值进行对比, 对比情况如图 7 所示, 图中各个数据点之间的线性度  $R^2=0.998$ 。可见, 测量得到的 CO 的体积分数与参考值的一致性较高, 二者具有良好的线性关系。图中实线是通过对散点图进行线性拟合得到的, 该拟合线斜率的大小为  $1.00282 \pm 0.02261$ , 可知实验系统测量误差保持在  $0.2\%$  左右, 由此验证了实验系统具有较高的测量准确性。

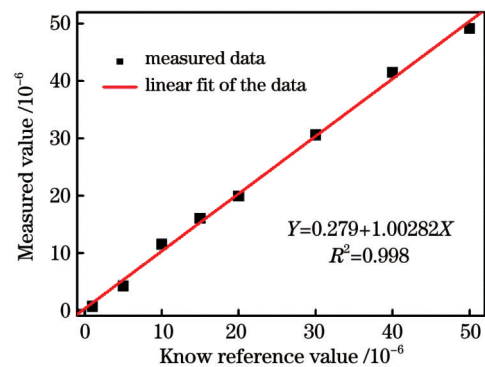


图 7 CO 体积分数测量值与已知参考值的对比

Fig. 7 Comparison between measured value and know reference value of CO volume fraction

### 5.2 系统对 CO 气体的探测极限分析

利用实验系统对 CO 体积分数为  $3 \times 10^{-6}$  的 CO+N<sub>2</sub> 混合气体进行了  $500 \text{ s}$  的时间序列测量, 每个数据的采样时间均为  $1 \text{ s}$ , 因此共得到  $500$  个数据点, 如图 8(a) 所示。图 8(b) 给出了  $500$  个数据点的直方图分布情况, 该直方图呈良好的高斯分布, 拟合曲线的半峰全宽 (HWHM) 可用于评价系统的测量精度。结果表明该系统对于 CO 体积分数的测量精度为  $286 \times 10^{-9}$ 。

利用 Allan 方差分析  $300 \text{ K}$ 、 $101325 \text{ Pa}$  条件下系统的探测灵敏度。在 CO 体积分数为  $3 \times 10^{-6}$  的条件

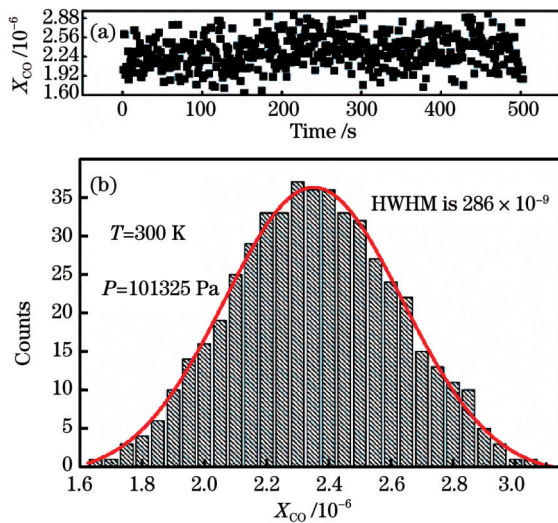


图 8 体积分数为  $3 \times 10^{-6}$  的 CO 的测量结果。(a) 连续测量结果; (b) 时间序列测量的直方图

Fig. 8 Measurement results of CO with volume fraction of  $3 \times 10^{-6}$ . (a) Successive measurement results; (b) histogram plot obtained from time series measurement

下,系统的 Allan 方差分析结果如图 9 所示。由图 9 可知在 1850 s 左右时 Allan 方差值最小,这代表该时间为系统的最佳探测时间,此时的探测极限可达  $138 \times 10^{-9}$ 。在最佳探测时间 1850 s 之前,系统的 Allan 方差值高于最低探测极限,这是由系统白噪声的影响造成的,而在 1850 s 之后的噪声主要是由系统的不稳定造成的。因此,在测量稳定流场时,可以在 1850 s 时间内通过对采集数据进行多次平均来降低噪声,提高测量精度。

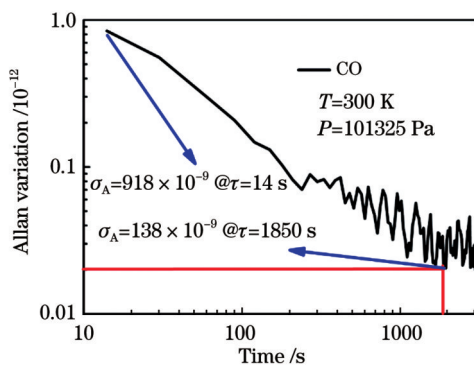


图 9 系统的 Allan 方差分析

Fig. 9 Allan variance analysis of the system

## 6 结 论

利用自制的密封箱搭建腔增强光谱测量系统,并选择  $4297.705 \text{ cm}^{-1}$  处的 CO 吸收谱线,基于腔增强吸收光谱技术和波长调制光谱技术,对 CO 进行了高灵敏度探测。通过标定得到了腔镜在  $2.3 \mu\text{m}$  处的反射率为 99.8%,与生产厂家所给数据一致;同时通过标定得到了该系统的有效吸收光程为 147.15 m,并确定了

最佳的调制振幅为 360 mV。实验过程中使用中心波长为  $2.3 \mu\text{m}$  的 DFB 激光器作为光源,在 101325 Pa、300 K 条件下,通过测量由 CO 与  $\text{N}_2$  配制的 CO 体积分数不同的混合气体的二次谐波信号,得到了各混合气体中 CO 的二次谐波信号的峰值高度与体积分数之间的线性关系,确定了在所测体积分数范围内二者具有良好的线性关系。将系统测量的 CO 体积分数与配气时的已知体积分数进行对比分析,得到系统的测量误差约为 0.2%,验证了所搭建系统的可靠性与准确性。最后对体积分数为  $3 \times 10^{-6}$  的 CO 气体的二次谐波信号进行测量,同时对系统的探测极限进行了分析,得到系统对 CO 的探测极限为  $138 \times 10^{-9}$ ,说明该系统对实际大气中的 CO 具有良好的探测性能。

## 参 考 文 献

- [1] 黄书华, 孙友文, 刘文清, 等. 基于非分散红外光谱吸收法的  $\text{SO}_2$  检测系统研究[J]. 红外, 2011, 32(12): 10-13.  
Huang S H, Sun Y W, Liu W Q, et al. Sulfur dioxide measurement system based on non-dispersive infrared gas analysis technique[J]. Infrared, 2011, 32(12): 10-13.
- [2] Pandey S K, Kim K H. The relative performance of NDIR-based sensors in the near real-time analysis of  $\text{CO}_2$  in air[J]. Sensors, 2007, 7(9): 1683-1696.
- [3] Tan T L, Lebron G B. Determination of carbon dioxide, carbon monoxide, and methane concentrations in cigarette smoke by Fourier transform infrared spectroscopy[J]. Journal of Chemical Education, 2012, 89(3): 383-386.
- [4] 李超, 李孟芝, 李丹霞, 等. 基于傅里叶变换红外光谱指纹技术的艾叶产地溯源研究[J]. 光谱学与光谱分析, 2022, 42(8): 2532-2537.  
Li C, Li M Z, Li D X, et al. Study on geographical traceability of *Artemisia argyi* by employing the Fourier transform infrared spectral fingerprinting[J]. Spectroscopy and Spectral Analysis, 2022, 42(8): 2532-2537.
- [5] 刘文清, 王兴平, 马国盛, 等. 高灵敏腔衰荡光谱技术及其应用研究[J]. 光学学报, 2021, 41(1): 0130003.  
Liu W Q, Wang X P, Ma G S, et al. Research of high sensitivity cavity ring-down spectroscopy technology and its application[J]. Acta Optica Sinica, 2021, 41(1): 0130003.
- [6] Maithani S, Pradhan M. Cavity ring-down spectroscopy and its applications to environmental, chemical and biomedical systems[J]. Journal of Chemical Sciences, 2020, 132(1): 114.
- [7] Xin F X, Li J, Guo J J, et al. Measurement of atmospheric  $\text{CO}_2$  column concentrations based on open-path TDLAS[J]. Sensors, 2021, 21(5): 1722.
- [8] Pan W D, Zhang J W, Dai J M, et al. Tunable diode laser absorption spectroscopy system for trace ethylene detection[J]. Spectroscopy and Spectral Analysis, 2012, 32(10): 2875-2878.
- [9] Lin S, Chang J, Sun J C, et al. Improvement of the detection sensitivity for tunable diode laser absorption spectroscopy: a review[J]. Frontiers in Physics, 2022, 10: 853966.
- [10] Li J S, Yu B L, Zhao W X, et al. A review of signal enhancement and noise reduction techniques for tunable diode laser absorption spectroscopy[J]. Applied Spectroscopy Reviews, 2014, 49(8): 666-691.
- [11] 姚路, 刘文清, 刘建国, 等. 基于 TDLAS 的长光程环境大气痕量 CO 监测方法研究[J]. 中国激光, 2015, 42(2): 0215003.  
Yao L, Liu W Q, Liu J G, et al. Research on open-path detection for atmospheric trace gas CO based on TDLAS[J]. Chinese Journal of Lasers, 2015, 42(2): 0215003.
- [12] 吴应发, 邱选兵, 李传亮, 等. 长光程大气湍流发生装置的设计

- 与性能测试[J]. 中国激光, 2015, 42(4): 0413004.
- Wu Y F, Qiu X B, Li C L, et al. Design and performance testing of long-optical-path atmospheric turbulence simulator[J]. Chinese Journal of Lasers, 2015, 42(4): 0413004.
- [13] 阚瑞峰, 刘文清, 张玉钧, 等. 可调谐二极管激光吸收光谱法监测大气痕量气体中的浓度标定方法研究[J]. 光谱学与光谱分析, 2006, 26(3): 392-395.
- Kan R F, Liu W Q, Zhang Y J, et al. Concentration calibration method of ambient trace-gas monitoring with tunable diode laser absorption spectroscopy[J]. Spectroscopy and Spectral Analysis, 2006, 26(3): 392-395.
- [14] Cho J H, Na S J. Implementation of real-time multiple reflection and Fresnel absorption of laser beam in keyhole[J]. Journal of Physics D: Applied Physics, 2006, 39(24): 5372-5378.
- [15] 黄伟, 高晓明, 邓伦华, 等. 1.315  $\mu\text{m}$  区域高分辨率水汽吸收光谱研究[J]. 光学学报, 2005, 25(2): 256-260.
- Huang W, Gao X M, Deng L H, et al. High-resolution absorption spectrum of water vapor near 1.315  $\mu\text{m}$ [J]. Acta Optica Sinica, 2005, 25(2): 256-260.
- [16] Xin P, Ming G, Ping C, et al. Cavity enhanced absorption spectroscopy of carbon dioxide using a DFB diode laser and a swept optical cavity[J]. Optica Applicata, 2004, 34(4): 589-595.
- [17] Guan S Y, Chen D B, Cao H L, et al. Study of a mode separation due to polarization existing in a cavity-enhanced absorption spectroscopy[J]. Sensors, 2021, 21(21): 7101.
- [18] 龙精明, 周卫东, 吴志伟. 基于 LabVIEW 的气体高分辨率光谱探测系统[J]. 中国激光, 2013, 40(1): 0115003.
- Long J M, Zhou W D, Wu Z W. A high sensitive spectral detection system of gaseous measurement based on LabVIEW[J]. Chinese Journal of Lasers, 2013, 40(1): 0115003.
- [19] 韩萃, 夏滑, 董凤忠, 等. 腔增强吸收光谱技术研究进展及其应用[J]. 中国激光, 2018, 45(9): 0911003.
- Han L, Xia H, Dong F Z, et al. Progress and application of cavity enhanced absorption spectroscopy technology[J]. Chinese Journal of Lasers, 2018, 45(9): 0911003.
- [20] Zhang L W, Zhang Z R, Sun P S, et al. A dual-gas sensor for simultaneous detection of methane and acetylene based on time-sharing scanning assisted wavelength modulation spectroscopy[J]. Spectrochimica Acta Part A: Molecular and Biomolecular Spectroscopy, 2020, 239: 118495.
- [21] Wang Z L, Chang J, Yu H S, et al. Multi-component and multi-point trace gas sensing in wavelength modulation spectroscopy based on wavelength stabilization[J]. Photonic Sensors, 2019, 9(4): 376-387.
- [22] Liang W K, Bi Y F, Zhou Q, et al. Developing  $\text{CH}_4$  detection limit at  $\lambda=1.654 \mu\text{m}$  by suppressing optical interference fringes in wavelength modulation spectroscopy[J]. Sensors and Actuators B: Chemical, 2018, 255: 2614-2620.
- [23] 王兴平, 彭冬, 李佳胜, 等. 基于波长调制吸收光谱的燃烧流场二维重建[J]. 中国激光, 2021, 48(7): 0711002.
- Wang X P, Peng D, Li J S, et al. Two-dimensional reconstruction of combustion flow field using wavelength-modulated absorption spectra[J]. Chinese Journal of Lasers, 2021, 48(7): 0711002.

## CO Volume Fraction Measurement Based on Wavelength Modulated Cavity-Enhanced Absorption Spectroscopy

Wang Xuan, Gao Guangzhen<sup>\*\*</sup>, Long Fangyu, Yang Yubing, Cai Tingdong<sup>\*</sup>

*School of Physics and Electronic Engineering, Jiangsu Normal University, Xuzhou 221116, Jiangsu, China*

### Abstract

**Objective** Based on cavity-enhanced absorption spectroscopy (CEAS) and wavelength modulated spectroscopy (WMS) technology, a cavity-enhanced spectrum measurement system was built to measure the volume fraction of CO gas. In an experiment, a distributed feedback laser (DFB) laser with a central wavelength of 2.3  $\mu\text{m}$  was used as the light source, and an optical cavity with a base length of 30 cm was constructed with two highly reflective mirrors with a reflectivity of 99.8%. An effective absorption path of 147.15 m was achieved. On this basis, CO was detected using the CO absorption spectral line at 4297.705  $\text{cm}^{-1}$  as the sensing target. In the experiment, the measurement accuracy of the system was verified using CO and  $\text{N}_2$  gas mixtures with different volume fractions of CO. The measured value was consistent with the reference value, and the measurement error was approximately 0.2%, which confirmed the measurement accuracy of the system. The detection limit of the system was analyzed using the second harmonic signal of CO gas with a volume fraction of  $3 \times 10^{-6}$ , and the lowest detectable CO volume fraction with the system was  $138 \times 10^{-9}$ .

**Methods** The optical cavity in the sealed box was composed of two highly reflective mirrors. The length of the cavity was 30 cm, diameter of the highly reflective mirrors specified by the manufacturer was 25.4 mm, and radius of curvature was 1 m. Their reflectivity reached 99.8% in a wavelength range of 1.9–2.3  $\mu\text{m}$ . In the experiment, the laser output from the 2.3  $\mu\text{m}$  DFB laser was divided into two parts using a fiber beam splitter. One part was passed through an oscilloscope (Bristol 671) to obtain the real-time scanning output wavelength of the laser, and the other part passed through the sealed box made of tempered glass. The laser beam entered the optical cavity through the sealed box. Then, after multiple reflections in the cavity, it was transmitted from the other end and converged in the InGaAs detector through a lens with focal length of 5 mm for detection. After the detector signal was sent to the input port of a lock-in amplifier, it demodulated the signal according to the specific setting parameters. The demodulated signal was collected by a data acquisition card (National Instruments USB-6361) and stored in the computer for subsequent data processing. A triangle wave with a frequency of 2 Hz generated by a function generator and a sine wave with a frequency of 880 Hz generated by a phase-locked amplifier were superimposed together by an adder, and the superimposed signal was sent to the laser controller to achieve scanning and modulation of the laser wavelength.

**Results and Discussions** The experiment was carried out under the fixed conditions of 101325 Pa and 300 K, and the second

harmonic ( $2f$ ) signals of different volume fractions of CO were measured. The  $2f$  signals of CO with volume fraction of  $3 \times 10^{-6}$ ,  $10 \times 10^{-6}$ ,  $30 \times 10^{-6}$ , and  $50 \times 10^{-6}$  are shown in Fig. 5. Figure 6 shows the linear relationship between the peak height of the  $2f$  signal of each volume fraction of CO and the volume fraction. The fitting results show that the linearity,  $R^2$ , between the data points was 0.998, while the relative standard deviation was 0.34%. It can be seen that the two maintained a good linear relationship within the volume fraction range measured in the experiment.

In this study, the measured CO volume fraction was compared with the known reference value during the gas distribution. This comparison is shown in Fig. 7. The linearity,  $R^2$ , between the data points in the figure was 0.998, which shows that the measured CO volume fraction was consistent with the reference value, and there was a good linear relationship between them. The red line in the figure was obtained by the linear fitting of the scatter plots. The slope of the fitting line was  $1.00282 \pm 0.02261$ . It can be seen that the measurement accuracy of the experimental system was maintained at approximately 0.2%, which confirmed that the measurement of the experimental system had high accuracy.

The system was used to conduct a 500 s time series measurement of CO gas with a volume fraction of  $3 \times 10^{-6}$ . Each data sampling time was 1 s. Thus, a total of 500 volume fraction points of CO gas were obtained, as shown in Fig. 8 (a). Figure 8 (b) shows the histogram distribution of the 500 data points. The histogram shows a good Gaussian distribution, and the half-height width (HWHM) of the curve could be used to evaluate the measurement accuracy of the system. The results show that the CO volume fraction measurement accuracy of the system was  $286 \times 10^{-9}$ . The Allan variance was used to analyze the detection sensitivity of the system under the environmental conditions of a temperature of 300 K and pressure of 101325 Pa, as shown in Fig. 9. It can be seen from the figure that when the system time was approximately 1850 s, the Allan variance was the lowest, which meant that this time was the best detection time for the system, and the detection limit at this time could reach  $138 \times 10^{-9}$ . Before the optimal detection time of 1850 s, the Allan variance of the system was higher than the minimum detection limit, which was due to the influence of the white noise of the system. The noise after this was mainly caused by the instability of the system. Therefore, when measuring a stable flow field, the noise could be reduced and the measurement accuracy could be improved by averaging the collected data for many measurements within a period of 1850 s.

**Conclusions** The CO absorption spectrum line at  $4297.705 \text{ cm}^{-1}$  was selected in the experiment. Based on cavity-enhanced absorption spectroscopy (CEAS) technology, combined with wavelength modulated spectroscopy (WMS) technology, a cavity-enhanced spectrum measurement system was built with a self-made sealed box. The reflectivity of the cavity mirror at  $2.3 \mu\text{m}$  was calibrated to be 99.8%, which was consistent with the data given by the manufacturer. At the same time, the effective absorption optical path of the system was calibrated to be 147.15 m, and the optimal modulation amplitude was determined to be 360 mV. During the experiment, a DFB laser with a central wavelength of  $2.3 \mu\text{m}$  was used as the light source. Under the conditions of 101325 Pa and 300 K, the linear relationship between the peak height of the  $2f$  signal of each each volume fraction of CO and the volume fraction was obtained by measuring the  $2f$  signals of the CO with different volume fractions prepared using the CO and  $\text{N}_2$  mixture gas, and a good linear relationship between the two was determined within the measured volume fraction range. Finally, the CO volume fraction measured by the system was compared with the known value during the gas distribution, and the measurement error was approximately 0.2%, which verified the reliability and accuracy of the system.

**Key words** spectroscopy; cavity-enhanced absorption spectroscopy; wavelength modulated spectrum; carbon monoxide gas; volume fraction measurement